Structure and function of bacterial YeeE-YeeD complex in thiosulfate uptake pathway

Authors

Mai Ikei[1,†], Ryoji Miyazaki[1,†], Keigo Monden[1], Yusuke Naito[1], Azusa Takeuchi[1], Yutaro S. Takahashi[1], Yoshiki Tanaka[1], Keina Murata[2], Takaharu Mori[2], Muneyoshi Ichikawa[3,*], Tomoya Tsukazaki[1,*]

Affiliations

[1]Division of Biological Science, Graduate School of Science and Technology, Nara Institute of Science and Technology, Ikoma, Nara 630-0192, Japan.

[2]Department of Chemistry, Faculty of Science, Tokyo University of Science, Shinjuku-ku, Tokyo 162-8601, Japan

[3]State Key Laboratory of Genetic Engineering, Department of Biochemistry and Biophysics, School of Life Sciences, Fudan University, Shanghai 200438, China.

[*]Corresponding author. Email: ichikawa_muneyoshi@fudan.edu.cn (M. Ichikawa); ttsukaza@bs.naist.jp (T.T.)

[†]These authors contributed equally to this work.

Abstract

Uptake of thiosulfate ions as an inorganic sulfur source from the environment is important for bacterial sulfur assimilation. Recently, a selective thiosulfate uptake pathway involving a membrane protein YeeE (TsuA) in *Escherichia coli* was characterized. YeeE-like proteins are conserved in some bacteria, archaea, and eukaryotes. However, the precise function of YeeE, along with its potential partner protein in the thiosulfate ion uptake pathway, remained unclear. Here, we assessed selective thiosulfate transport via *Spirochaeta thermophila* YeeE in vitro and characterized *E. coli* YeeD (TsuB) as an adjacent and essential protein for YeeE-mediated thiosulfate uptake in vivo. We further showed that *S. thermophila* YeeD possesses thiosulfate decomposition activity and that a conserved cysteine in YeeD was modified to several forms in the presence of thiosulfate. Finally, the crystal structures of *S. thermophila* YeeE-YeeD fusion proteins at 3.34-Å and 2.60-Å resolutions revealed their interactions. The association was evaluated by a binding

assay using purified *S. thermophila* YeeE and YeeD. Based on these results, a model of the sophisticated uptake of thiosulfate ions by YeeE and YeeD is proposed.

125-character sentence

The structural study of the YeeE-YeeD membrane protein complex provides insight into the thiosulfate uptake and degradation mechanism.

INTRODUCTION

From bacteria to eukaryotes, sulfur is a vital element for cellular activities. For example, sulfur-containing biomolecules, such as L-cysteine, L-methionine, thiamine, glutathione, and biotin, play a variety of essential roles in cells (*1*). Bacteria and plants can utilize L-cysteine as a source of sulfate, but they also have sulfur assimilation pathways to synthesize L-cysteine from inorganic sulfur compounds. In bacteria, L-cysteine is important not only as a component for protein synthesis but also as a reducing agent against oxidative stress (*2*). There are two pathways for bacterial L-cysteine synthesis, which use O-acetylserine as a precursor, called the sulfate and thiosulfate pathways (*3*). In the sulfate pathway, sulfate ion is first decomposed into sulfide ion through phosphorylation by two molecules of ATP and reduction by four molecules of NADPH. Subsequently, L-cysteine is synthesized from sulfide ion and O-acetylserine by O-acetylserine sulfhydrylase-A (CysK). In the thiosulfate pathway, S-sulfocysteine is synthesized from thiosulfate ion and O-acetylserine by O-acetylserine sulfhydrylase-B (CysM); S-sulfocysteine is then reduced by one NADPH molecule, and L-cysteine is synthesized. The sulfate and thiosulfate ions used in these pathways are taken up from the environment by transporters on the cytoplasmic membrane. Sulfate and thiosulfate ions are trapped by periplasmic proteins Sbp (*4*) and CysP (*5*), respectively. Both sulfate and thiosulfate ions are then passed on to a complex formed by the inner membrane proteins CysU and CysW and the cytosolic protein CysA (CysUWA) (also called CysTWA) (*3*) and transported into the cytoplasm by the CysUWA complex using the energy from ATP hydrolysis.

A bacterial membrane protein, YeeE, has been identified as mediating thiosulfate uptake based on growth complementation assay of *Escherichia coli* cells, and the structure of *Spirochaeta thermophila* YeeE (*St*YeeE) has been determined by X-ray crystallography (*6*). YeeE was proposed to be almost entirely buried in the membrane and shows a unique hourglass-like structure. An electron density near a conserved cysteine residue on the outside surface was assigned to a thiosulfate ion, which seemed to be connected to the sulfur atom of the cysteine via a S─H─S hydrogen bond (*6*). In addition, the binding of thiosulfate ions to purified YeeE protein was shown by isothermal titration calorimetry experiments. In the center of YeeE, three conserved, functionally important cysteines, including the thiosulfate-interacting one, are arranged side by side and perpendicular to the membrane. Based on these structural features and in vivo functional

analysis using a series of mutants, thiosulfate ion was proposed to be transported from the environment to the cytoplasm while transiently interacting with the three conserved cysteine residues by relays mediated via hydrogen bonds (*6*), independently of the thiosulfate pathway described above. However, it has not been elucidated whether YeeE alone transports thiosulfate ions. Moreover, no YeeE-associated protein has been clearly defined, although one candidate gene is *yeeD*, which resides within the same operon that includes *yeeE* (*7*), and the regulatory mechanism of the alternative, sophisticated thiosulfate uptake by YeeE remains unclear.

Recently, in addition to the *E. coli yeeE* gene, *yeeD* was shown to be involved in thiosulfate uptake and the two were named *tsuA* and *tsuB*, respectively (*8*). YeeD is a cytoplasmic protein that belongs to the TusA (tRNA 2-thiouridine synthesizing protein A) protein family (*9*). TusA plays various roles in sulfate transfer activities in cells, such as thiomodification of tRNA (*10*), molybdenum cofactor biosynthesis (*11*), and dissimilatory sulfur and tetrathionate oxidation (*12*). The cysteine residue in a Cys-Pro-X-Pro (CPxP) motif of TusA receives activated sulfur from the L-cysteine desulfurase IscS (*13*). Although YeeD possesses the CPxP motif, it cannot complement TusA function (*11*). Therefore, YeeD is thought to have a sulfate-related yet distinct function from TusA in bacteria. In some bacteria, such as Gram-positive *Corynebacterium* species YeeE and YeeD are encoded as one polypeptide, implying that they function together in the thiosulfate uptake pathway. However, the enzymatic activity of YeeD and the functional cooperativity of YeeE and YeeD have not been well characterized.

In this study, first, we measured thiosulfate uptake activity using *St*YeeE-reconstituted liposomes to clarify YeeE function. Second, according to an *E. coli* growth complementation assay, we found that *E. coli* YeeD (*Ec*YeeD) plays an essential role in YeeE function in vivo. Third, we demonstrated a thiosulfate decomposition activity in purified *S. thermophila* YeeD (*St*YeeD). Fourth, direct interaction between *St*YeeE and *St*YeeD proteins was detected, and substrate thiosulfate ions weakened the binding of these proteins. Fifth, the crystal structures of *St*YeeE–YeeD complex were determined at 3.34-Å and 2.60-Å resolutions. Critical residues of YeeD for both its activity and interaction with YeeE were defined. Based on these results, detailed mechanisms for the functional cooperation between YeeE and YeeD in thiosulfate uptake are discussed.

RESULTS

YeeE-mediated thiosulfate transport

Although *E. coli* growth complementation tests showed that YeeE is involved in the uptake of thiosulfate ions (*6*), thiosulfate transport via YeeE has not yet been demonstrated. To detect thiosulfate uptake activity using a purified reconstituted system, we adapted solid-supported membrane (SSM)-based electrophysiology (*14*). First, *St*YeeE-reconstituted liposomes were applied to the SSM, and charge displacement was measured in the presence of sulfate ions or thiosulfate ions (Fig. 1A). A change in the potential toward the negative direction was observed in the presence of thiosulfate ions but not sulfate ions, meaning that negatively charged thiosulfate ions were selectively transported into the proteoliposomes. The slight change in the potential toward the positive direction in the presence of sulfate ions was probably due to buffer shock since there was no counter ion present in these measurements. Next, because *St*YeeE-reconstituted liposomes showed no transport activity for sulfate ions, we measured YeeE activity using sulfate as a counter ion. As a result, a clear peak toward the negative direction (-0.62 nA) was observed only in the presence of *St*YeeE (Fig. 1B). The negative peak area increased when higher concentrations of thiosulfate ions were used (Fig. 1C). These experiments verified that YeeE transports thiosulfate ions specifically but not sulfate ions.

YeeD is essential for the YeeE-mediated thiosulfate pathway

According to recent reports (*7, 8*), YeeD may function in combination with YeeE in *E. coli*. YeeD is composed of about 80 amino acid residues and possesses one or two cysteines, which are highly conserved among bacteria. In some organisms, such as *E. coli*, YeeD has two conserved cysteine residues (C13 and C39 in *Ec*YeeD), while other organisms like *S. thermophila* have one conserved cysteine residue (C17 in *St*YeeD) (Fig. 2A). The invariant cysteine residue in the N-terminal region is part of a CPxP motif that is conserved among TusA family proteins (Fig. 2A and fig. S1). The predicted *Ec*YeeD structure in the AlphaFold2 database (*15, 16*) shows a globular shape with two α-helices and a β-sheet composed of four β-strands (Fig. 2B), similar to other TusA protein structures (*17, 18*). To evaluate the influence of YeeD on YeeE activity in cells, a growth complementation assay using *E. coli* MG1655 *ΔcysPUWA ΔyeeE::kan* (DE3) cells was performed, as described previously (*6*). These *E. coli* cells, which lack sulfate and

137 thiosulfate ion-uptake pathways, cannot grow in the presence of thiosulfate as a sole
138 sulfur source (Fig. 2C and fig. S2, A and B), but can when they carry a plasmid containing
139 the *E. coli yeeE* operon, which includes *yeeE* and *yeeD* (*6*) (Fig. 2C). When the *yeeD*
140 region was deleted, growth was similar to the negative control, which was conducted
141 using a vector without *yeeE* and *yeeD* regions (Fig. 2C), revealing that YeeD is essential
142 for thiosulfate uptake via YeeE in vivo. Further, we prepared a series of alanine mutations
143 in *Ec*YeeD, including the conserved cysteine mutations C13A and C39A, that are located
144 on the surface of the AlphaFold2 model (Fig. 2B). Subsequent growth complementation
145 assays using these YeeD mutations demonstrated the significance of C13 and C39, but
146 not of the other mutated residues (E19, K21, E26, D31, E32, and D38), in *Ec*YeeD
147 function (Fig. 2C).
148
149 **Thiosulfate decomposition activity of YeeD and its catalytic center residue**
150 To unveil the enzymatic function of YeeD itself, we purified *St*YeeD and its mutant
151 proteins and then conducted their biochemical analyses in vitro. The gel filtration profile
152 of purified His-tagged *St*YeeD(WT) (11.3 kDa) appears to be a mixture of dimers and
153 monomers as compared to gel filtration markers (fig. S2C), similar to TusA (*12*). Non-
154 reducing and reducing SDS-PAGE after the addition of iodoacetamide (IAA) or N-
155 Ethylmaleimide (NEM), which block the sidechain of Cys residues, showed that almost
156 all *St*YeeD(WT) lacks disulfide bond formation: the dimeric *St*YeeD apparent in gel
157 filtration profiles is not due to disulfide bond formation (fig. S2D). In the range of 10–15
158 kDa on SDS-PAGE gels, purified *St*YeeD(WT) exhibited main and faint minor bands,
159 whereas *St*YeeD(C17A), a putative catalytic center mutant, exhibited only the main band
160 (Fig. 2, D and E). Since this slightly upshifted band did not disappear even in reducing
161 SDS-PAGE (fig. S2D), the -SH group might be modified to an irreversible oxidation state.
162 Indeed, oxidation of WT *St*YeeD with hydrogen peroxide significantly increased the
163 reductant-resistant band (fig. S2E), presumably due to irreversible formation of sulfinic
164 acid ($-SO_2^-$) or sulfonic acid ($-SO_3^-$) (*19*). To examine *St*YeeD modification at C17, we
165 performed matrix-assisted laser desorption ionization-time of flight (MALDI-TOF) mass
166 spectrometry (MS) of YeeD in several conditions. The samples for MS were prepared
167 under aerobic conditions. The spectrum of purified YeeE in the absence of thiosulfate
168 revealed three major peaks with m/z of 11317.3, 11349.7, and 11394.3 (Fig. 2D). The
169 first peak (11317.3 m/z) was assigned as unmodified *St*YeeD (-SH at C17) as its

170 theoretical m/z value is 11315.7. The second peak (11349.7 m/z) might correspond to
171 sulfinic acid (-S-O_2^- at C17) and/or persulfide modification (-S-S^- at C17) as it increased
172 by 32.4 (close to the value of 2 oxygen atoms, 32.0, or 1 sulfur atom, 32.1). Although the
173 formation of sulfinic acid (see above) may be an artifact due to oxidation in the
174 purification process, the persulfide modification was also found by MS in purified
175 *Pseudomonas aeruginosa* PA1006, an ortholog of *E. coli* TusA (*20*), which has one
176 conserved cysteine residue corresponding to C17 of *St*YeeD. The third 77.0 m/z-
177 increased peak (11394.3 m/z) may be attributable to perthiosulfonic acid (-S-SO_3^- at C17).
178 In contrast, *St*YeeD(C17A) showed only one prominent peak (11283.4 m/z) as its
179 theoretical unmodified value (11283.6 m/z) (Fig. 2E). These results suggest that the C17
180 of *St*YeeD is highly reactive to sulfur-related molecules and susceptible to sulfur(S_γ)-
181 related modifications. Next, we performed MS analysis of the *St*YeeD protein in the
182 presence of DL-Dithiothreitol (DTT), a reductant. The third peak entirely disappeared
183 after the addition of DTT (Fig. 2F). By contrast, the second peak remained even in the
184 presence of DTT. Persulfide modification (-S-S^-) can be reduced by DTT (*20*) but sulfinic
185 acid (-S-O_2^-), an overoxidation product, is irreversible as previously shown (*19, 21*).
186 Therefore, in the DTT condition, the second peak is thought to be residual sulfinic acid
187 product. Using sample treated with DTT, to gain insights into catalytic intermediates, MS
188 analysis was performed in the presence of thiosulfate (Fig. 2G). In the condition with
189 thiosulfate (500 μM), a peak with m/z value of 11431.0 appeared. The peak with an m/z
190 value of 11431.0 may correspond to -S-$S_2O_3^-$ because the m/z increments were equivalent
191 to the addition of S_2O_3 to StYeeD(-SH). The previously reported crystal structure of
192 TsdBA (PDB ID 5LO9) included the same modification of a cysteine residue's thiol (-
193 SH) group to -S-$S_2O_3^-$, indicating that this modification is one of the stable forms (*22*). In
194 the case of StYeeD(C17A), the addition of thiosulfate did not increase the m/z (Fig. 2E).
195 In addition, we performed MS using *St*YeeD sample treated with DTT and then hydrogen
196 peroxide (Fig. 2H). In this condition, the peak corresponding to *St*YeeD(-SH) completely
197 disappeared, but peaks corresponding to sulfinic acid (-S-O_2^-), sulfonic acid (-S-O_3^-), and
198 perthiosulfonic acid (-S-SO_3^-) were observed. Given these results, although
199 perthiosulfonic acid (-S-SO_3^-) detected in the purified StYeeD is thought to be due to
200 oxidization during the purification procedure, *St*YeeD may temporarily take the -S-SO_3^-
201 form in the process of thiosulfate decomposition.

202 The additional binding of S_2O_3 to the C17 side chain, in form of -S-$S_2O_3^-$, and
203 the existence of persulfide modification (-S-S^- at C17) and perthiosulfonic acid (-S-SO_3^-
204 at C17), as indicated by the MS results, raise the possibility that YeeD decomposes
205 thiosulfate ion ($S_2O_3^{2-}$) and releases sulfide ion (S^{2-}). To test this, we monitored hydrogen
206 sulfide (H_2S) derived from thiosulfate-decomposed sulfide ions using a fluorescent probe
207 for H_2S, HSip-1. A significant increase in fluorescence intensity was observed in the
208 presence of *St*YeeD compared with an irrelevant protein, BSA, and with no protein (Fig.
209 2I and fig. S2G), suggesting that YeeD catalyzes the decomposition of thiosulfate as a
210 substrate. We also tested the thiosulfate decomposition activity of several *St*YeeD
211 mutants. Among these, only C17A did not show a significant increase in fluorescence;
212 NEM-modified *St*YeeD also did not. These results indicated that the conserved cysteine
213 residue of YeeD (C17 in *St*YeeD) is the catalytic center residue for thiosulfate
214 decomposition.
215
216 **Crystal structure of the YeeE-YeeD complex**
217 We succeeded in crystallizing a fusion protein of *St*YeeE and *St*YeeD, designed based on
218 the amino acid sequence of *Corynebacterium pollutisoli* YeeED, which is expressed as a
219 single protein. First, because a comparison of *St*YeeE/D and several YeeEDs' amino acid
220 sequences revealed that *C. pollutisoli* YeeED possesses the shortest linker, of 40 amino
221 acids, between its YeeE and YeeD regions, we prepared the fusion protein by introducing
222 the 40 residues between the C-terminus of *St*YeeE and the N-terminus of *St*YeeD. Second,
223 after attempting but failing to crystallize the fusion protein, *St*YeeE-*St*YeeD, we tried
224 crystallization using alanine mutants of the conserved cysteines in *St*YeeE-*St*YeeD and
225 succeeded in crystallizing *St*YeeE(C22A)-*St*YeeD. Using the X-ray diffraction dataset of
226 *St*YeeE(C22A)-*St*YeeD, we determined the crystal structure of the *St*YeeE-*St*YeeD
227 complex at 3.34 Å (fig. S3A,B, and Table 1 8J4C). However, the resolution was
228 insufficient to reveal the details of the interactions between YeeE and YeeD. Introducing
229 a mutation in YeeD (L45A) strengthened the interaction, as found in binding experiments
230 using purified YeeE and YeeD mutants (described later). The diffraction dataset of
231 crystals of *St*YeeE(C22A)-*St*YeeD(L45A) was improved to 2.60 Å (Fig. 3A and Table 1
232 8K1R), and the resulting 2.60 Å crystal structure enabled us to discuss the detailed
233 interactions between YeeE and YeeD.

234 Each crystal lattice in the datasets was the same, except for having slightly
235 different unit cell dimensions (Table 1). The asymmetric unit contains two molecules of
236 *St*YeeED, Mol A and Mol B. In the crystal packing, *St*YeeD in Mol A is involved in
237 interacting with an adjacent YeeD region, but YeeD in Mol B is not (fig S3A). When the
238 two *St*YeeE-*St*YeeD structures (Mol A and Mol B), showing different packing
239 interactions, were superimposed, the crystal structures were almost identical with an
240 RSMD of 0.433 Å for 8J4C or 0.155 Å for 8K1R for Cα atoms (fig. S3A). Although the
241 orientation of YeeD relative to YeeE is slightly different, the RMSD between 8J4C and
242 8K1R for Cα atoms is 0.896 (fig. S3C) and the active site of YeeD is similar. Therefore,
243 in this paper, we introduce Mol A of the higher resolution structure, which shows the best
244 electron density map, to explain YeeE and YeeD interactions.
245 The overall structure of YeeE in the crystal structure of *St*YeeE-*St*YeeD
246 resembles the previously reported crystal structure of *St*YeeE (PDB ID 6LEP) (*6*), with
247 an RMSD of 0.596 Å for Cα atoms (fig. S3D). The cytoplasmic indentation of *St*YeeE
248 associates with *St*YeeD, which consists of two α-helices and four β-sheets. The
249 architecture of *St*YeeD is similar in shape to the sequence-homologous *E. coli* TusA (22.5%
250 identical) (PDB ID 3LVK) (fig. S3E) (*18*). Residues involved in the YeeE-YeeD
251 interaction are shown in Fig. 3B. C22 of *St*YeeE is located at the interface, implying that
252 C22A affects the interaction. Residues R28, R98, E101, and E261 on the cytoplasmic
253 surface, conserved in YeeEs (*6*), were found to be involved in the interaction with YeeD.
254 While the important, conserved residues C293, C91, and C22, termed the first, second,
255 and third cysteines, respectively, are arranged perpendicular to the membrane at 8.6- and
256 6.7-Å intervals, C17 of *St*YeeD, one of the YeeE-interacting residues, is the putative
257 enzymatic active site and is located adjacent to C22 of *St*YeeE as the "fourth cysteine".
258 This positioning means that a thiosulfate ion transported through the membrane via the
259 center region of YeeE interacts with the first-to-third cysteines of YeeE in succession and
260 then interacts with the fourth cysteine of YeeD. The distance between the third and the
261 fourth cysteines, 10.8 Å, is wider than that between the other cysteines, and this space
262 may be needed for transient binding of the thiosulfate ion rather than its transport (Fig.
263 3C). A water molecule is located at position III, a predicted thiosulfate-binding site (6).
264 A position where another water molecule is located below position III corresponds to the
265 position of the side chain of C22 (6). The relay of a thiosulfate ion from position III to
266 C17 is likely facilitated by the conserved positively charged residues R28 and R98 (Fig.

267 3C). The CPxP motif forms a cis peptide between C17 and P18 and is located at the
268 beginning of the α-helix (Fig. 3D), similar to a previous report (*17*). In addition, the
269 electron density of the peptide bonds between V16 and C17 is faint, which may be closely
270 related to C17 being the active center.
271
272 **Interaction between YeeE and YeeD.**
273 To confirm that the interactions between YeeE and YeeD revealed in the crystal structures
274 of *St*YeeE-YeeD fusion protein also occur in solution, we performed a binding assay
275 based on the bio-layer interferometry (BLI) method (*23*) using purified *St*YeeE and His-
276 tagged *St*YeeD. Clear association and dissociation of *St*YeeE with an *St*YeeD-solidified
277 Ni-NTA sensor were observed as real-time wavelength shifts (Fig. 4A, blue). Based on
278 the *St*YeeE binding-dependent wavelength changes, the K_D between *St*YeeD and *St*YeeE
279 was estimated as 1.6 ± 0.20 μM. When a buffer containing sulfate ion was used, the
280 binding was similar to that in a buffer without a sulfur source (fig. S4, A and B). In
281 contrast, *St*YeeE showed significantly decreased binding to *St*YeeD in a buffer containing
282 thiosulfate ions (fig. S4, A and B). We next sought the important residues for the
283 interaction using a series of *St*YeeD mutants (fig. S2F). The mutants E15A, V16A, C17A,
284 D42A, Y43A, E48A, and R49A severely impaired *St*YeeD's affinity for *St*YeeE. while
285 the mutant L45A enhanced the affinity (Fig. 4B). This enhanced affinity could stabilize
286 the crystal packing of *St*YeeE-*St*YeeD, leading to its higher-resolution structure. In the
287 crystal structure, most of these influential residues for affinity were located at the border
288 region between YeeE and YeeD (Fig. 4C). On the other hand, Ala substitutions on the
289 opposite side maintained affinity (Fig. 4). The calculated K_a, K_d and K_D values for YeeD
290 mutant proteins are summarized in Table 2. Notably, the conserved cysteine residue (C17)
291 of *St*YeeD proved to be pivotal for not only the enzyme activity but also the interaction
292 with *St*YeeE. These BLI results in solution are consistent with the crystal structure.
293 To further assess the important residues of YeeE for the interaction with YeeD,
294 we used a growth complementation assay. *Ec*YeeE mutations of residues at the
295 interaction surface (R21A, R101A, E104A, E271A, R275A) could not complement the
296 growth of *E. coli* MG1655 *ΔcysPUWA ΔyeeE::kan* (DE3) cells (fig. S4, C and D). These
297 results emphasize that the interaction of YeeE and YeeD is essential for in vivo function
298 of thiosulfate uptake.
299

300 **MD simulation of YeeE/YeeD complex.**

301 In the presence of thiosulfate ions, *St*YeeD was easily modified (Fig. 2G) and the binding
302 between *St*YeeE and *St*YeeD decreased (fig. S4A, B), leading to the hypothesis that the
303 modified *St*YeeD dissociates from *St*YeeE. Here, to address how the *St*YeeE-YeeD
304 complex undergoes structural changes when *St*YeeD is in the YeeD-SH or YeeD-S-$S_2O_3^-$
305 states, we conducted molecular dynamics (MD) simulation analysis (fig. S5). In the case
306 of *St*YeeD-SH, no significant structural changes were observed during the 1-μs MD
307 simulation (fig. S5A): the simulation structure remained similar to the crystal structure of
308 the *St*YeeE-YeeD complex (PDB ID 8K1R) (fig. S5C). On the other hand, in the case of
309 *St*YeeD-S-$S_2O_3^-$, the *St*YeeD root mean square deviations (RMSD) for C-alpha atoms
310 increased from around 400 ns; in other words, *St*YeeD moved away from the cytoplasmic
311 concave surface of *St*YeeE (fig. S5A–C). The calculation results are consistent with the
312 idea that the interaction between YeeE and YeeD weakens upon Cys-modifications of
313 YeeD. The dissociation of YeeD from YeeE may facilitate the release of thiosulfate ions'
314 decomposition products from the Cys positions of YeeD into the cytoplasm.

315

316 **DISCUSSION**

317 By the growth complementation assay, we have demonstrated that YeeD is a required
318 enzyme for growth when thiosulfate is solely imported via YeeE. YeeD's substrate was
319 identified as the thiosulfate ion, and the uptake activity for thiosulfate ions was measured
320 using YeeE-reconstituted liposomes. In addition, the interaction between YeeE and YeeD
321 was revealed by both binding assay and X-ray crystallography. By mutational analysis of
322 YeeD, a conserved cysteine residue was found to be critical for YeeE's activity in vivo
323 as well as thiosulfate ion decomposition activity.

324 Compared with other TusA family proteins, YeeD shows some similarities and
325 differences. Although conserved cysteine residues in other TusA family proteins,
326 corresponding to C17 in *St*YeeD, are important for their own activities (*10, 20*), TusA
327 could not decompose thiosulfate ions (*24*). *Metallosphaera cuprina* TusA was reported
328 to exist as both monomer and dimer forms (*12*). Similarly, *St*YeeD appeared to be
329 monomers and dimers in gel filtration (fig. S2C). *St*YeeD may exploit this feature to
330 transiently form a dimer in the thiosulfate decomposition reaction (discussed below). The
331 conserved cysteine residues in YeeD and TusA are important for binding to their
332 respective partners (Fig. 4) (*12, 18*), which seems to be a common feature in TusA family

333 proteins. Meanwhile, YeeD is unique in that its interaction partner, YeeE, is a membrane
334 protein, unlike other TusA family proteins. Previously, the conserved cysteine residue of
335 PA1006 was reported to be persulfide-modified (*20*). Furthermore, *St*YeeD has several
336 different sulfur-related modification statuses, including persulfide modification,
337 perthiosulfonic acid, and thiosulfonate (Fig. 2, D, F–H). In the case of DsrE3 and TusA,
338 the conserved cysteines can possess thiosulfonate, but the modifications were detected
339 only with their substrate tetrathionate (*12*). Along with the fact that YeeE only allows
340 thiosulfate to pass through, YeeD also seems to be specialized for thiosulfate reactivity.
341 Both can contribute to the efficient uptake of thiosulfate. Since YeeE alone can transport
342 thiosulfate ions but was unable to rescue the growth deficiency in vivo, cooperation
343 between YeeE and YeeD is crucial. In this study, we have unveiled a sophisticated
344 pathway for thiosulfate uptake in the bacterial membrane. An open question is whether
345 there are other proteins that directly receive sulfur compounds from YeeD in sulfur
346 assimilation pathways.
347 Based on our findings, we propose detailed mechanisms for thiosulfate ion
348 uptake by YeeE and YeeD (Fig. 5A). From the previous crystal structure of *St*YeeE, the
349 transportation of thiosulfate ions across the membrane was proposed to be relayed by the
350 first-to-third cysteine residues (*6*). Our crystal structure of the *St*YeeE and *St*YeeD
351 complex now further shows that YeeD is positioned to interact with the YeeE cytoplasmic
352 side, which we propose to be the exit of the thiosulfate pathway on YeeE; the conserved
353 cysteine residue of YeeD can function as a "fourth cysteine". Therefore, the interactions
354 between the two can facilitate the delivery of a thiosulfate ion from YeeE to YeeD: the
355 conserved cysteine residue of YeeD can directly capture a thiosulfate ion passed through
356 YeeE. This transport scheme of thiosulfate ions by YeeE and YeeD recalls a group-
357 translocation originally proposed by Mitchell and Moyle (*25*). From our X-ray crystal
358 structure, YeeE and YeeD appear to work as a 1:1 complex. The fact that YeeE and YeeD
359 are encoded as a single polypeptide in some species supports this idea. After receiving
360 the thiosulfate ion, YeeD's conserved cysteine would be thiosulfonated. Our BLI method
361 analysis in the presence of thiosulfate showed that the interaction between *St*YeeD and
362 *St*YeeE was weakened, possibly due to thiosulfonation on YeeD. The thiosulfonated
363 YeeD may therefore dissociate from YeeE and be released into the cytoplasm. This
364 dissociation model agrees well with our MD simulation results. Since YeeD can
365 decompose thiosulfate by itself, it would do so after dissociating from YeeE. Of

366 additional note, since the existence of *St*YeeD dimers in solution was suggested by gel
367 filtration chromatography, *St*YeeD may form a transient dimer after being released from
368 *St*YeeE.

369 We suggest a plausible mechanism for decomposition of thiosulfate ion by
370 YeeD (Fig. 5B). While the reducing power for this series of reactions is thought to be
371 supplied from the cytoplasm, a reducing environment, the electron route remains
372 unknown and needs to be elucidated in a future study. In the presence of thiosulfate ion,
373 *St*YeeD incorporated thiosulfate, but *St*YeeD(C17A) did not (Fig. 2E and G), suggesting
374 that the thiosulfate ion directly binds to the cysteine residue of YeeD. Our MS results also
375 suggest that there are *St*YeeD molecules with perthiosulfonic acid (-S-SO_3^-) and
376 persulfide modifications (-S-S^-). Taking this together with the detection of H_2S in the
377 presence of *St*YeeD and thiosulfate ion (Fig. 2H), it would be reasonable for sulfide ion
378 (S^{2-}) to be released from a persulfide-modified version of *St*YeeD (-S-S^-) (Fig. 5B).
379 Although sulfonic acid (-SO_3^-) formation by the oxidization of a cysteine residue is an
380 irreversible process, perthiosulfonic oxidization of a cysteine residue (-S-SO_3^-) is
381 reversible as shown by Doka et al. (*19*). Therefore, even if -S-SO_3^- is formed, sulfite ion
382 (SO_3^{2-}) will be released. In our experimental condition for the thiosulfate decomposition
383 assay, reductant β-ME is present to facilitate these reactions. In the cell, there could be
384 other acceptor proteins which take S or SO_3 atoms from YeeD protein. Such proteins
385 should be identified in a future study. While the significance of the *St*YeeD dimer in this
386 study has not been demonstrated, if it were involved in this series of reactions, the scheme
387 depicted in the Fig. 5 box would likely occur. Because *St*YeeD does not form disulfide
388 bonds in its dimer (fig. S2C and D), one StYeeD molecule in a dimer can be
389 thiosulfonated and the other can have an active -SH group, which can take the SO_3 from
390 thiosulfonated YeeD (-S-$S_2O_3^-$). Through this process, a persulfide-modified form (-S-S^-)
391 can be generated. In some bacteria, including *E. coli*, YeeD has two cysteine residues. In
392 species having YeeD with two cysteine residues, the above-mentioned process could be
393 carried out by one YeeD molecule using these two cysteine residues. Another possibility
394 is that the non-conserved cysteine (C39) of *Ec*YeeD may not serve as the decomposition
395 active center, but may interact with YeeE and/or enhance its activity. In agreement with
396 these ideas, our growth complementation assay showed that both cysteines are important
397 for the growth of *E. coli* cells.

398 In the 2.60-Å structure of *St*YeeE-*St*YeeD, the electron density is faint on the
399 N-terminal side of the CPxP motif, raising the possibility that some electrons may be
400 attracted to the CPxP motif (Fig. 3D). If that happens, the CPxP motif could make the
401 region electron-rich and exhibit high reducing power. Previously, the CPxP architecture
402 was proposed to stabilize an α-helix-1 by capping it (*17*). In the TusA family proteins,
403 the formation of CPxP may also provide high reducing power, conferring on them the
404 unique property of selective decomposition of their substrates.
405 In conclusion, we revealed that YeeE and YeeD cooperatively contribute to the
406 thiosulfate uptake pathway and possess unprecedented regulation mechanisms. Our
407 findings also deepen the understanding of the functions of TusA family proteins.
408
409 **MATERIALS AND METHODS**
410 **Strains and plasmids**
411 For the growth complementation assay, we used plasmids derived from pAZ061, which
412 is based on pET-16b-TEV (*26*) and possesses *E. coli yeeE* and *yeeD* genes between
413 BamHI and XhoI sites amplified from *E. coli* genomic DNA (JCM 20135, RIKEN BRC)
414 using primer set 5′-
415 AAATTTATATTTTCAAGGATCCCATATGTTTTCAATGATATTAAG-3′ and 5′-
416 GGCTTTGTTAGCAGCCCTCGAGTCAGGCTTTTTGAACGG-3′ (fig. S2A), and the
417 *E. coli* MG1655 *ΔcysPUWA ΔyeeE::kan* (DE3) strain, which cannot grow on a minimum
418 medium with thiosulfate ion as the single sulfur source (*6*). pAZ061 derivatives having
419 mutations in the *yeeD* region were prepared by site-directed mutagenesis. The DNA
420 sequence encoding *Ec*YeeD was deleted from pAZ061 using primers 5′-
421 GTTTGGGTTAGGCATCGCTTCCCCAACGGCC-3′ and 5′-
422 GGCCGTTGGGGAAGCGATGCCTAACCCAAAC-3′.
423 The plasmid used to express *St*YeeE (1-328aa, UniProt ID: G0GAP6) with C-
424 terminal GSSGENLYFQGEDVE-His_8 sequence (pKK550) was prepared as in (*6*). For
425 the expression of the *St*YeeE-*St*YeeD fusion protein, we modified pKK550; the resulting
426 plasmid, pAZ150, encodes *St*YeeE (1–330 aa)-
427 AATPTPVAEAAPSSAEDRVLPFQVATGAVALQTAPRVKKA-*St*YeeD (1–80 aa,
428 UniProt ID: G0GAP7)-GSSGENLYFQGEDVE-His_6. The mutations in the *St*YeeE and
429 *St*YeeD regions were introduced by site-directed mutagenesis.

430 For the expression of *St*YeeD, the DNA sequence encoding *St*YeeD (1–80 aa)
431 was inserted into a modified pCGFP-BC plasmid. The resulting plasmid, pNT015,
432 expresses *St*YeeD (1–80 aa)- GSSGENLYFQGEDVE-His_6. The pNT015 derivatives
433 were prepared by Gene Synthesis and Mutagenesis (SC1441, GenScript) or site-directed
434 mutagenesis.
435
436 **Growth complementation tests of *E. coli* cells**
437 *E. coli* MG1655 *ΔcysPUWA ΔyeeE::kan* (DE3) cells harboring pAZ061 or its derivatives
438 were cultured in LB medium containing 50 μg/ml ampicillin and 25 μg/ml kanamycin for
439 16 h at 37 °C. The culture was diluted 100-fold and cultured for another 8 h at 37 °C,
440 after which the cells were precipitated by centrifugation and washed twice with S-free
441 medium (42 mM Na_2HPO_4, 22 mM KH_2PO_4, 8.6 mM NaCl, 19 mM NH_4Cl, 1 mM $MgCl_2$,
442 0.2% (w/v) glucose, 0.01% (w/v) thiamine hydrochloride, and 0.1 mM $CaCl_2$).
443 Subsequent passage cultures in S-free medium containing 500 μM $Na_2S_2O_3$ were started
444 at OD_{600} = 0.2. The ΔOD_{600} of the culture was measured every 30 min with OD-Monitor
445 C&T (TAITEC) for 24 h. Measurement was performed three times for each transformant.
446
447 **Protein expression and purification**
448 *St*YeeE and *St*YeeE(C22A)-*St*YeeD proteins were purified as follows. *E. coli* C41(DE3)
449 cells transformed with plasmids expressing these proteins were cultured in 2.5 l of LB
450 medium containing 50 μg/ml ampicillin until the OD_{600} reached 0.4. Isopropyl β-D-
451 thiogalactopyranoside (IPTG) was then added to 1 mM, and the cells were cultured at
452 30 °C for 17 h. Subsequent procedures were performed at 4 °C or on ice. The cells were
453 collected by centrifugation as pellets, suspended in a buffer (10 mM Tris-HCl pH 8.0,
454 300 mM NaCl, 1 mM EDTA-Na pH 8.0, 2 mM $Na_2S_2O_3$, 0.1 mM phenylmethylsulfonyl
455 fluoride (PMSF), and 1 mM β–mercaptoethanol (β-ME)), and disrupted with a
456 Microfluidizer Processor M-110EH (Microfluidics International). The suspension was
457 centrifuged (10,000 rpm for 20 min, himac R13A rotor), and the collected supernatant
458 was further ultracentrifuged (40,000 rpm for 60 min, Beckman 45Ti rotor) to obtain the
459 membrane fraction, which was flash-frozen in liquid nitrogen and stored at -80 °C until
460 purification. The membrane fraction was resuspended in solubilization buffer (20 mM
461 Tris-HCl pH 8.0, 300 mM NaCl, 2 mM $Na_2S_2O_3$, 10 mM imidazole-HCl pH 8.0, 5% (v/v)
462 glycerol, 1 mM β-ME, 0.1 mM PMSF) containing 1% (w/v) n-dodecyl β-maltoside

463 (DDM) and stirred at 4 °C for 60 min. The insoluble fraction was removed by
464 ultracentrifugation (45,000 rpm for 30 min, Beckman 70Ti rotor), and the supernatant
465 was mixed with 5 ml of Ni-NTA agarose (QIAGEN) pre-equilibrated with solubilization
466 buffer for 60 min. Then, 100 ml of wash buffer (20 mM Tris-HCl pH 8.0, 300 mM NaCl,
467 2 mM $Na_2S_2O_3$, 50 mM imidazole-HCl pH 8.0, 5% (v/v) glycerol, 1 mM β-ME, 0.1 mM
468 PMSF, 0.1% (w/v) DDM) was added to the column. Next, 5 ml of elution buffer (20 mM
469 Tris-HCl pH 8.0, 300 mM NaCl, 2 mM $Na_2S_2O_3$, 200 mM imidazole-HCl pH 8.0, 5%
470 (v/v) glycerol, 1 mM β-ME, 0.1 mM PMSF, and 0.1% (w/v) DDM) was added to the
471 column six times, and the fractions with target proteins were pooled. To remove the His-
472 tag, TEV(S219V) protease (*27*) was added with a protein weight ratio of 10 (proteins):1
473 (TEV) and the protein solution was dialyzed overnight against dialysis buffer (20 mM
474 Tris-HCl pH 8.0, 300 mM NaCl, 2 mM $Na_2S_2O_3$, 0.1% (w/v) DDM, 1 mM β-ME). Ni-
475 NTA agarose (2.5 ml) pre-equilibrated with dialysis buffer was added to the sample and
476 stirred for 60 min to remove TEV proteases. The flow-through fraction was collected,
477 concentrated with an Amicon Ultra 50K NMWL (Merck Millipore), and ultracentrifuged
478 (45,000 rpm for 30 min, himac S55A2 rotor). The sample was then applied to a Superdex
479 200 increase 10/300 GL column (Cytiva) equilibrated with a buffer (20 mM Tris-HCl pH
480 8.0, 300 mM NaCl, 2 mM $Na_2S_2O_3$, 0.1% (w/v) DDM, 1 mM β-ME). The fractions with
481 target proteins were collected and pooled. *St*YeeE(C22A)-*St*YeeD(L45A) protein was
482 purified as for *St*YeeE and *St*YeeE(C22A)-YeeD except that the buffer lacked $Na_2S_2O_3$.
483 *St*YeeD purification was performed as follows. *E. coli* C41(DE3) cells containing
484 *St*YeeD-encoding plasmids were inoculated into 25 ml of LB medium containing 50
485 μg/ml ampicillin and cultured overnight at 37 °C. The culture was then added to 0.5 l of
486 LB medium containing 50 μg/ml ampicillin and allowed to grow until OD_{600} = 0.4. After
487 the addition of IPTG to 1 mM, the cells were cultured at 30 °C for 17 h. The cells were
488 collected by centrifugation (4,500 rpm for 10 min, himac R9A2), flash-frozen in liquid
489 nitrogen, and stored at -80 °C until use. The next procedures were performed at 4 °C or
490 on ice. The frozen pellets were suspended in 25 ml of sonication buffer (20 mM Tris-HCl
491 pH 8.0, 300 mM NaCl, 10 mM imidazole-HCl pH 8.0, 1 mM β-ME, 0.1 mM PMSF),
492 sonicated for 10 min on ice with a Q500 sonicator (QSONICA), and centrifuged (15,000
493 rpm for 30 min, himac R13A). Ni-NTA agarose (2.5 ml) pre-equilibrated with the
494 sonication buffer was added to the supernatant and rotated for 1 h. After the flow-through
495 fraction was removed, the resin was washed with 125 ml of a buffer (20 mM Tris-HCl

496 pH 8.0, 300 mM NaCl, 20 mM imidazole-HCl pH 8.0, 1 mM β-ME, 0.1 mM PMSF).
497 Next, 5 ml of a buffer (20 mM Tris-HCl pH 8.0, 300 mM NaCl, 200 mM imidazole-HCl
498 pH 8.0, 1 mM β-ME, 0.1 mM PMSF) was added, and the elution fraction was collected.
499 The elution step was repeated six times. The fractions with target proteins were pooled
500 and concentrated using an Amicon Ultra 3K NMWL (Merck Millipore). The sample was
501 ultracentrifuged (45,000 rpm x 30 min, himac S55A2 rotor) and loaded onto a Superdex
502 200 increase 10/300 GL column pre-equilibrated with YeeD gel filtration buffer (10 mM
503 Tris-HCl pH 8.0 and 300 mM NaCl). The fractions with *St*YeeD proteins were
504 concentrated using an Amicon Ultra 3K NMWL.
505
506 **MALDI-TOF MS**
507 For *St*YeeD(WT) sample preparation for MS (Fig. 2D), *St*YeeD(WT) protein was mixed
508 with gel filtration buffer, so that the final concentration of *St*YeeD(WT) was 48.2 μM and
509 the total volume was 200 μl, and incubated for 2.5 h at 37 °C. The sample was then
510 ultracentrifuged, and the buffer was exchanged with MS buffer (10 mM Tris-HCl pH 8.0)
511 using a NAP-5 Column (Cytiva). The final concentration of *St*YeeD(WT) for MS analysis
512 was 17.5 μM.
513 For *St*YeeD(C17A) sample preparation for MS (Fig. 2E), 48.2 μM
514 *St*YeeD(C17A) in gel filtration buffer was incubated with or without 500 μM thiosulfate
515 for 2.5 h at 37 °C in a total volume of 200 μl. After the incubation, the sample was
516 ultracentrifuged, and the buffer was exchanged with MS buffer using a NAP-5 Column.
517 The final concentrations of *St*YeeD(C17A) were 12.3 μM for without thiosulfate and 16.6
518 μM for with thiosulfate.
519 For the DTT condition of *St*YeeD(WT) (Fig.2F), DTT was added to
520 *St*YeeD(WT) to give final concentrations of 401 μM and 16.7 mM, respectively, and a
521 total volume of 288 μl. The sample was then incubated for 10 min at 37 °C and
522 ultracentrifuged. A 48-μl aliquot was taken and the buffer was exchanged with MS buffer
523 using a NAP-5 Column. The concentration of resultant DTT-treated *St*YeeD(WT) was
524 10.96 μM. For the thiosulfate or hydrogen peroxide condition of *St*YeeD(WT), the DTT-
525 treated *St*YeeD(WT) sample was processed as follows. First, to remove DTT, the sample
526 was applied to a Superdex 200 Increase 10/300 GL column (Cytiva) pre-equilibrated with
527 gel filtration buffer. Next, the sample after gel filtration was concentrated using Amicon
528 ultra 3K NMWL. For the thiosulfate condition (Fig. 2G), the sample was then mixed with

529 thiosulfate so that the final concentrations of *St*YeeD(WT) and thiosulfate were 48.2 μM
530 and 500 μM, respectively, and the total volume was 200 μl. After incubating for 2.5 h at
531 37 °C, the sample was ultracentrifuged, and the buffer was exchanged with MS buffer
532 using a NAP-5 Column. The final concentration of *St*YeeD(WT) for MS analysis was
533 14.0 μM. For the hydrogen peroxide condition (Fig. 2H), the sample after gel filtration
534 and concentration was mixed with hydrogen peroxide so that the final concentrations of
535 *St*YeeD(WT) and hydrogen peroxide were 48.2 μM and 0.1% (w/v), respectively, and the
536 total volume was 200 μl. After incubating for 10 min at room temperature, the sample
537 was ultracentrifuged, and the buffer was exchanged with MS buffer using a NAP-5
538 Column. The final concentration of *St*YeeD(WT) for MS analysis was 23.8 μM.
539 Samples for MALDI-TOF analysis were prepared by the sinapinic acid (SA)
540 double layer method (*28*). In brief, 1 μl matrix solution A (saturated solution of SA in
541 ethanol) was deposited onto the MALDI target and allowed to dry. Matrix solution B
542 (saturated solution of SA in TA30 solvent (1:2 (v/v) acetonitrile:0.1% (v/v)
543 trifluoroacetic acid in water)) and protein solution were mixed at a ratio of 1:24 (v/v).
544 Matrix solution B/protein mixture was then deposited onto the matrix spot and allowed
545 to dry. The dried samples were analyzed by Autoflex-II (Bruker Daltonics) with a linear
546 positive mode and acquisition mass range of 3,000–20,000 Da. Theoretical m/z values
547 were calculated with the equation of m/z = (M + n)/n, where M is molecular mass and n
548 is the charge (n = 1 was adopted).
549
550 **Measurement of enzyme activity of *St*YeeD**
551 The release of H_2S due to chemical decomposition of thiosulfate ions by *St*YeeD was
552 monitored by HSip-1 (Dojindo, SB21-10). The reaction solution contained 19.6 μM
553 HSip-1, 24.1 μM YeeD, and 70 μM β-ME in the YeeD gel filtration buffer. As negative
554 controls, 24.1 μM BSA was used instead of YeeD, or no protein was added to the solution.
555 The reaction was started by adding 5 μl of 100 mM $Na_2S_2O_3$ at a 1:200 [v/v] ratio (final,
556 500 μM $Na_2S_2O_3$), and the solution was incubated at 37 °C. The fluorescence of HSip-1
557 was measured using a fluorescence spectrophotometer (F-7000, Hitachi), at an excitation
558 wavelength of 491 nm and an emission wavelength of 521 nm, every 30 min until 150
559 min.
560
561 **Crystallization**

562 Purified *St*YeeE(C22A)-*St*YeeD fusion protein was concentrated to 21.5 mg/ml by
563 Amicon Ultra 50K NMWL and crystallized using the lipidic cubic phase (LCP) method,
564 as previously performed in the case of purified *St*YeeE (*6*). Fifteen microliters of 21.5
565 mg/ml *St*YeeE(C22A)-*St*YeeD was mixed with 4.3 µl of a buffer (20 mM Tris-HCl pH
566 8.0, 300 mM $Na_2S_2O_3$, 0.1% (w/v) DDM, 1 mM β-ME) and incubated on ice for 20 min.
567 Then, 16 µl of the sample was mixed with 24 µl of monoolein (M-239, Funakoshi) in an
568 LCP syringe (Art Robbins Instruments) for 10 min. After 30 min of incubation at 20°C,
569 30 nl of the mixed samples were spotted onto MRC under oil crystallization plates
570 (Hampton Research) using the Crystal Gryphon protein crystallization aliquot system
571 (Art Robbins Instruments) with 3 µl of buffers (18 to 24% (v/v) pentaerythritol-
572 propoxylate (5/4 PO/OH), 100 mM 2-morpholinoethanesulfonic acid (MES)-NaOH pH
573 7.0, and 300 mM NaCl) covering them. The plate was incubated at 20 °C for 7 days. For
574 *St*YeeE(C22A)-*St*YeeD(L45A) fusion protein, the purified protein was concentrated to
575 16.5 mg/ml and crystallized using the LCP method. The crystals appeared using 0.35 M
576 ammonium formate, 0.1 M Tris-HCl (pH 8.0 to 9.0), and 22 to 42% (v/v) 1,4-Butanediol
577 as covering solutions. The plate was incubated at 20 °C for 14 days. The crystals that
578 appeared were harvested by Crystal Mounts and Loops (MiTegen) without using
579 cryoprotectant, directly flash-frozen in liquid nitrogen, and stored in liquid nitrogen until
580 X-ray diffraction experiments.
581
582 **Data collection and structural determination**
583 X-ray diffraction experiments of *St*YeeE(C22A)-*St*YeeD and *St*YeeE(C22A)-
584 *St*YeeD(L45A) were performed at beamline BL32XU of SPring-8. Data were collected
585 with the automated data collection system ZOO (*29*). The complete data sets were
586 obtained by combining multiple small wedge datasets from hundreds of tiny crystals with
587 sizes of approximately 20 µm. The principle of this method has been described in detail
588 (*30*). Data processing was performed with KAMO (*30*) using XDS (*31*) programs. For
589 *St*YeeE(C22A)-*St*YeeD dataset, the initial phase was determined by molecular
590 replacement using the *St*YeeE crystal structure (PDB ID: 6LEO) as a template by
591 PHASER (*32*), and a *St*YeeD structure predicted by AlphaFold2 (*15, 16*) was manually
592 fitted to the density map using COOT (*33*). Structure refinement was performed using
593 COOT (*33*) and PHENIX (*34*) iteratively until R_{work}/R_{free} reached 0.265/0.310 at 3.34 Å
594 resolution. For *St*YeeE(C22A)-*St*YeeD(L45A) dataset, the initial phase was determined

595 by molecular replacement using the *St*YeeE(C22A)-*St*YeeD structure as a template by
596 MOLREP (*35*). Refinement of the structure was performed using COOT (*33*) and
597 PHENIX (*34*) in a iterative way until R_{work}/R_{free} reached 0.206/0.255 at 2.60 Å resolution.
598 Figures of the structures were prepared using PyMOL (https://pymol.org/2/) and Chimera
599 (*36*).
600
601 **Interaction analysis between *St*YeeE and *St*YeeD by the BLI method**
602 BLI method (*23*) was performed to analyze the interaction between *St*YeeE and *St*YeeD-
603 His_6 proteins using the Octet N1 System (Sartorius) at room temperature. A Ni-NTA
604 biosensor was hydrated with Octet buffer (20 mM Tris-HCl pH 8.0, 300 mM NaCl, 0.1%
605 (w/v) DDM, 1 mM β-ME) for 10 min and mounted in the Octet N1 System. The biosensor
606 was first dipped in Octet buffer, and the initial baseline was measured for 30 sec. Next,
607 the biosensor was dipped in 4.82 μM *St*YeeD-His_6 protein solution in Octet buffer for
608 120 sec for loading. The solution was then changed to Octet buffer for 30 sec to measure
609 the baseline, after which, the biosensor was submerged in 11.05 μM *St*YeeE solution in
610 Octet buffer for 120 sec to measure the association of *St*YeeE. Finally, the buffer was
611 exchanged to Octet buffer, and the dissociation of *St*YeeE from the biosensor was
612 measured for 120 sec. Biosensors without *St*YeeD-His_6 proteins were measured with the
613 same procedure and used as references. After the reference data were subtracted from
614 *St*YeeD-His_6 protein data, the association rate constant (k_a), dissociation rate constant (k_d),
615 and affinity constant (K_D) were calculated by a local fitting method. Measurements were
616 performed three times for each protein.
617
618 **Reconstitution of proteoliposomes**
619 A mixture of 0.8 mg/ml *St*YeeE and 4 mg/ml *E. coli* total lipid extract (Avanti Polar
620 Lipids) in a buffer (20 mM HEPES-HCl pH 7.0, 300 mM NaCl, 5% (v/v) glycerol, and
621 0.1% (w/v) DDM) was rotated at 4 °C for 1 h. Next, the detergent was removed using
622 SM2-beads (Bio-Rad). The resulting solution was ultracentrifuged, and the precipitates
623 were suspended in a buffer (25 mM HEPES-NaOH pH 7.5 and 100 mM NaCl). The
624 reconstituted proteoliposome samples were flash-frozen in liquid nitrogen and stored at -
625 80 °C until measurements.
626
627 **Measurement of ion transport activity**

628 The SSM method was used to detect thiosulfate uptake activity of the *St*YeeE-
629 reconstituted proteoliposomes. Frozen proteoliposomes were thawed on ice and sonicated
630 using a bath sonicator (VELVO-CLEAR, VS-50R) for 10 s three times before use.
631 Measurement was performed using SURFE^{2}R N1 (Nanion Technologies) as described
632 (*14*). First, 50 µl of 0.5 mM 1-octadecanethiol (dissolved in isopropanol) was applied to
633 N1 Single Sensors (Nanion Technologies, Nr. 2-03-35002-000) and incubated for 30 min
634 at room temperature. Next, the sensors were washed twice with isopropanol, washed
635 twice with distilled water, and dried. Then, 1.5 µl of 7.5 µg/µl 1,2-diphytanoyl-sn-
636 glycero-3-phosphocholin (dissolved in n-decane) was applied to the sensor, followed by
637 50 µl of non-activating buffer (B buffer: 140 mM NaCl, 4 mM $MgCl_2$, 25 mM HEPES,
638 25 mM MES, KOH pH 6.7, with or without Na_2SO_4). Proteoliposomes were pipetted
639 toward the sensor beneath the B buffer surface, and the sensor was centrifuged (2,000*g*
640 for 30 min, 25 °C) to adsorb the liposomes onto the sensor surface. The resultant sensors
641 were mounted in SURFE^{2}R N1, and the sensors were rinsed with buffer B before each
642 measurement. The current change on the sensor was monitored while B buffer and A
643 buffer (140 mM NaCl, 4 mM $MgCl_2$, 25 mM HEPES, 25 mM MES, KOH pH 6.7, with
644 $Na_2S_2O_3$) were exchanged. For each condition, measurement was performed four times,
645 and the three results with least noise were analyzed.
646
647 **MD simulations of *St*YeeE-*St*YeeD complex**
648 All-atom MD simulations of the StYeeE-StYeeD complex were performed in
649 POPE/POPG mixed lipid bilayers and 150 mM NaCl solution, where two intermediate
650 states, *St*YeeE-*St*YeeD-SH and *St*YeeE-*St*YeeD-S-$S_2O_3^-$, were examined. The initial
651 structure of the protein–membrane complex was constructed using the CHARMM-GUI
652 *membrane builder* (*37*). The system size is 100 Å × 100 Å × 120 Å, and the total number
653 of atoms is ~111,600. The CHARMM C36m force field parameters were used for proteins
654 and lipids (*38*), and the topology and parameters for S-$S_2O_3^-$-modified Cys were derived
655 from the CGenFF parameters (*39*). The system was equilibrated using 2,000-step energy
656 minimization, followed by equilibration in the *NVT* and *NPT* ensembles for 3.5 ns using
657 the positional restraints on the proteins and lipids. The production run was then carried
658 out for 1 µs in the *NPT* ensemble at T = 310 K and P = 1 atm with the time step of 3.5 fs
659 using the RESPA integrator with hydrogen-mass repartitioning and bond-length
660 constraining (*40*) and the Bussi thermostat and barostat for temperature and pressure

661 control (*41*). The particle-mesh Ewald method was used for the calculation of long-range
662 electrostatic interaction (*42*). All simulations were performed using GENESIS (*43, 44*).
663

664 **REFERENCES AND NOTES**

665 1. A. Francioso, A. Baseggio Conrado, L. Mosca, M. Fontana, Chemistry and Biochemistry of
666 Sulfur Natural Compounds: Key Intermediates of Metabolism and Redox Biology. *Oxid Med*
667 *Cell Longev* **2020**, 8294158 (2020).
668 2. G. D. Westrop, G. Goodall, J. C. Mottram, G. H. Coombs, Cysteine biosynthesis in Trichomonas
669 vaginalis involves cysteine synthase utilizing O-phosphoserine. *J Biol Chem* **281**, 25062-25075
670 (2006).
671 3. T. Nakatani *et al.*, Enhancement of thioredoxin/glutaredoxin-mediated L-cysteine synthesis from
672 S-sulfocysteine increases L-cysteine production in Escherichia coli. *Microb Cell Fact* **11**, 62
673 (2012).
674 4. C. T. Pereira, C. Roesler, J. N. Faria, M. R. Fessel, A. Balan, Sulfate-Binding Protein (Sbp) from
675 Xanthomonas citri: Structure and Functional Insights. *Mol Plant Microbe Interact* **30**, 578-588
676 (2017).
677 5. A. Sirko, M. Hryniewicz, D. Hulanicka, A. Bock, Sulfate and thiosulfate transport in Escherichia
678 coli K-12: nucleotide sequence and expression of the cysTWAM gene cluster. *J Bacteriol* **172**,
679 3351-3357 (1990).
680 6. Y. Tanaka *et al.*, Crystal structure of a YeeE/YedE family protein engaged in thiosulfate uptake.
681 *Sci Adv* **6**, eaba7637 (2020).
682 7. B. K. Mohanty, S. R. Kushner, Inactivation of RNase P in Escherichia coli significantly changes
683 post-transcriptional RNA metabolism. *Mol Microbiol* **117**, 121-142 (2022).
684 8. S. Morigasaki, A. Umeyama, Y. Kawano, Y. Aizawa, I. Ohtsu, Defect of RNA
685 pyrophosphohydrolase RppH enhances fermentative production of L-cysteine in Escherichia
686 coli. *J Gen Appl Microbiol* **66**, 307-314 (2021).
687 9. T. Yamashino, M. Isomura, C. Ueguchi, T. Mizuno, The yhhP gene encoding a small ubiquitous
688 protein is fundamental for normal cell growth of Escherichia coli. *J Bacteriol* **180**, 2257-2261
689 (1998).
690 10. Y. Ikeuchi, N. Shigi, J. Kato, A. Nishimura, T. Suzuki, Mechanistic insights into sulfur relay by
691 multiple sulfur mediators involved in thiouridine biosynthesis at tRNA wobble positions. *Mol*
692 *Cell* **21**, 97-108 (2006).

693 11. J. U. Dahl *et al.*, The sulfur carrier protein TusA has a pleiotropic role in Escherichia coli that
694 also affects molybdenum cofactor biosynthesis. *J Biol Chem* **288**, 5426-5442 (2013).
695 12. L. J. Liu *et al.*, Thiosulfate transfer mediated by DsrE/TusA homologs from acidothermophilic
696 sulfur-oxidizing archaeon Metallosphaera cuprina. *J Biol Chem* **289**, 26949-26959 (2014).
697 13. T. S. Tanabe, S. Leimkuhler, C. Dahl, The functional diversity of the prokaryotic sulfur carrier
698 protein TusA. *Adv Microb Physiol* **75**, 233-277 (2019).
699 14. A. Bazzone, M. Barthmes, K. Fendler, SSM-Based Electrophysiology for Transporter Research.
700 *Methods Enzymol* **594**, 31-83 (2017).
701 15. M. Varadi *et al.*, AlphaFold Protein Structure Database: massively expanding the structural
702 coverage of protein-sequence space with high-accuracy models. *Nucleic Acids Res* **50**, D439-
703 D444 (2022).
704 16. J. Jumper *et al.*, Highly accurate protein structure prediction with AlphaFold. *Nature* **596**, 583-
705 589 (2021).
706 17. E. Katoh *et al.*, High precision NMR structure of YhhP, a novel Escherichia coli protein
707 implicated in cell division. *J Mol Biol* **304**, 219-229 (2000).
708 18. R. Shi *et al.*, Structural basis for Fe-S cluster assembly and tRNA thiolation mediated by IscS
709 protein-protein interactions. *PLoS Biol* **8**, e1000354 (2010).
710 19. E. Doka *et al.*, Control of protein function through oxidation and reduction of persulfidated
711 states. *Sci Adv* **6**, eaax8358 (2020).
712 20. G. Tombline *et al.*, Pseudomonas aeruginosa PA1006 is a persulfide-modified protein that is
713 critical for molybdenum homeostasis. *PLoS One* **8**, e55593 (2013).
714 21. B. Ezraty, A. Gennaris, F. Barras, J. F. Collet, Oxidative stress, protein damage and repair in
715 bacteria. *Nat Rev Microbiol* **15**, 385-396 (2017).
716 22. J. M. Kurth *et al.*, Electron Accepting Units of the Diheme Cytochrome c TsdA, a Bifunctional
717 Thiosulfate Dehydrogenase/Tetrathionate Reductase. *J Biol Chem* **291**, 24804-24818 (2016).
718 23. Y. Abdiche, D. Malashock, A. Pinkerton, J. Pons, Determining kinetics and affinities of protein
719 interactions using a parallel real-time label-free biosensor, the Octet. *Anal Biochem* **377**, 209-
720 217 (2008).
721 24. Y. Stockdreher *et al.*, New proteins involved in sulfur trafficking in the cytoplasm of
722 Allochromatium vinosum. *J Biol Chem* **289**, 12390-12403 (2014).
723 25. P. Mitchell, J. Moyle, Group-translocation: a consequence of enzyme-catalysed group-transfer.
724 *Nature* **182**, 372-373 (1958).

725 26. Y. Daimon *et al.*, The TPR domain of BepA is required for productive interaction with substrate
726 proteins and the beta-barrel assembly machinery complex. *Mol Microbiol* **106**, 760-776 (2017).
727 27. R. B. Kapust *et al.*, Tobacco etch virus protease: mechanism of autolysis and rational design of
728 stable mutants with wild-type catalytic proficiency. *Protein Eng* **14**, 993-1000 (2001).
729 28. Y. Dai, R. M. Whittal, L. Li, Two-layer sample preparation: a method for MALDI-MS analysis
730 of complex peptide and protein mixtures. *Anal Chem* **71**, 1087-1091 (1999).
731 29. K. Hirata *et al.*, ZOO: an automatic data-collection system for high-throughput structure analysis
732 in protein microcrystallography. *Acta Crystallogr D Struct Biol* **75**, 138-150 (2019).
733 30. K. Yamashita, K. Hirata, M. Yamamoto, KAMO: towards automated data processing for
734 microcrystals. *Acta Crystallogr D Struct Biol* **74**, 441-449 (2018).
735 31. W. Kabsch, Xds. *Acta Crystallogr D Biol Crystallogr* **66**, 125-132 (2010).
736 32. A. J. McCoy *et al.*, Phaser crystallographic software. *J Appl Crystallogr* **40**, 658-674 (2007).
737 33. P. Emsley, B. Lohkamp, W. G. Scott, K. Cowtan, Features and development of Coot. *Acta*
738 *Crystallogr D Biol Crystallogr* **66**, 486-501 (2010).
739 34. P. V. Afonine *et al.*, Towards automated crystallographic structure refinement with
740 phenix.refine. *Acta Crystallogr D Biol Crystallogr* **68**, 352-367 (2012).
741 35. A. Vagin, A. Teplyakov, Molecular replacement with MOLREP. *Acta Crystallogr D Biol*
742 *Crystallogr* **66**, 22-25 (2010).
743 36. E. F. Pettersen *et al.*, UCSF Chimera--a visualization system for exploratory research and
744 analysis. *J Comput Chem* **25**, 1605-1612 (2004).
745 37. E. L. Wu *et al.*, CHARMM-GUI Membrane Builder toward realistic biological membrane
746 simulations. *J Comput Chem* **35**, 1997-2004 (2014).
747 38. J. Huang *et al.*, CHARMM36m: an improved force field for folded and intrinsically disordered
748 proteins. *Nat Methods* **14**, 71-73 (2017).
749 39. K. Vanommeslaeghe *et al.*, CHARMM general force field: A force field for drug-like molecules
750 compatible with the CHARMM all-atom additive biological force fields. *J Comput Chem* **31**,
751 671-690 (2010).
752 40. J. Jung *et al.*, Optimized Hydrogen Mass Repartitioning Scheme Combined with Accurate
753 Temperature/Pressure Evaluations for Thermodynamic and Kinetic Properties of Biological
754 Systems. *J Chem Theory Comput* **17**, 5312-5321 (2021).
755 41. G. Bussi, D. Donadio, M. Parrinello, Canonical sampling through velocity rescaling. *J Chem*
756 *Phys* **126**, 014101 (2007).

42. U. Essmann *et al.*, A smooth particle mesh Ewald method. *The Journal of Chemical Physics* **103**, 8577-8593 (1995).
43. J. Jung *et al.*, GENESIS: a hybrid-parallel and multi-scale molecular dynamics simulator with enhanced sampling algorithms for biomolecular and cellular simulations. *Wiley Interdiscip Rev Comput Mol Sci* **5**, 310-323 (2015).
44. C. Kobayashi *et al.*, GENESIS 1.1: A hybrid-parallel molecular dynamics simulator with enhanced sampling algorithms on multiple computational platforms. *J Comput Chem* **38**, 2193-2206 (2017).
45. X. Robert, P. Gouet, Deciphering key features in protein structures with the new ENDscript server. *Nucleic Acids Res* **42**, W320-324 (2014).

Acknowledgments: We thank Kayo Abe for secretarial assistance, Akira Sasaki for liposome preparation, Rie Kurata for performing mass spectrometry, Naoki Sakai for helping with the data analysis, the beamline scientists at BL32XU of SPring-8 (Hyogo, Japan) for helping with data collection, and Nanion Technologies for assistance with initial data collection. The synchrotron radiation experiments were performed at BL32XU of SPring-8 with the approval of the Japan Synchrotron Radiation Research Institute (JASRI) (Proposal Nos. 2020A2564, 2021A2745, 2022A2738, 2023A2727). **Funding:** This work was supported by JSPS/MEXT KAKENHI (Grant No. 21H05157 to T.M., Grant Nos. JP22K15075, JP20K15733 to M. Ichikawa, Grant No. JP22K15061, JP22H05567 to R.M., and Grant Nos. JP22H02567, JP22H02586, JP21H05155, JP21H05153, JP21K19226, JP21KK0125 to T.T.), MEXT as "Program for Promoting Researches on the Supercomputer Fugaku" (Development and application of large-scale simulation-based inferences for biomolecules JPMXP1020230119) and HPCI project (hp200064 and hp230209) to T.M., PRESTO (JPMJPR20E1 to M. Ichikawa) from the Japan Science and Technology Agency (JST), and private research foundations (the Chemo-Sero-Therapeutic Research Institute, Naito Foundation, Takeda Science Foundation, G-7 Scholarship Foundation, the Sumitomo Foundation, the Institute for Fermentation (Osaka), Yamada Science Foundation, KOSÉ Cosmetology Research Foundation, and Japan Foundation for Applied Enzymology) to T.T. *E. coli* JCM20135 was provided by RIKEN BRC, which is participating in the National Bio-Resources Project of MEXT, Japan. **Author Contributions:** Conceptualization, A.T., M. Ichikawa, and T.T.; Methodology and investigation, M. Ikei, R.M., K. Monden, Y.N., A.T., Y.S.T.,

Y.T., K. Murata, T.M., M. Ichikawa, and T.T.; Writing – original draft, M. Ichikawa and T.T.; Writing, review & editing, M. Ichikawa and T.T.; Supervision, M. Ichikawa and T.T. **Competing interests:** The authors declare no competing interests. **Data and materials availability:** Coordinates and structure factors have been deposited in the Protein Data Bank under accession number 8J4C and 8K1R. All data needed to evaluate the conclusions in the paper are present in the paper and/or the Supplementary Materials. Additional data related to this paper may be requested from the authors.

FIGURES AND TABLES

Table 1. Data collection and refinement

Statistics for the highest-resolution shell are shown in parentheses.

PDB ID		8J4C	8K1R
Crystal		*St*YeeE(C22A)-*St*YeeD	*St*YeeE(C22A)-*St*YeeD(L45A)
Data Collection			
X-ray source		SPring-8 BL32XU	SPring-8 BL32XU
Wavelength (Å)		1.00	1.00
Space group		$P2_122_1$	$P2_122_1$
a, b, c (Å)		73.98, 102.44, 186.52	73.58, 101.75, 182.76
Resolution range (Å)		47.60–3.34 (3.46–3.34)	49.01–2.60 (2.69–2.60)
Total reflections		432750 (38159)	13803448 (1256177)
Unique reflections		21249 (2011)	42977 (4206)
Multiplicity		20.4 (18.4)	321.2 (297.1)
Completeness (%)		99.04 (96.87)	99.52 (99.32)
$I/\sigma(I)$		4.12 (0.83)	15.25 (2.10)
Wilson B-factor		49.19	31.95
R-pim		0.2207 (1.017)	0.0478 (0.2706)
$CC_{1/2}$		0.963 (0.578)	0.996 (0.861)
Refinement			
Reflections used in refinement		21070 (2011)	42846 (4206)
Reflections used for R-free		1990 (190)	1993 (196)
R_{work}		0.2654 (0.3596)	0.2064 (0.2705)
R_{free}		0.3095 (0.4113)	0.2547 (0.3108)
Number of non-hydrogen atoms		6675	6900
protein		6238	6247
thiosulfate		10	0
monoolein		427	545
water		0	108
RMS derivations	bond length (Å)	0.003	0.009
	bond angles (°)	0.56	1.16
MolProbity Validation	overall score	1.95	1.80
	clashscore	11.91	7.67
	rotamer outliers (%)	0.00	1.72
Ramachandran	favoured (%)	94.80	96.77
	allowed (%)	4.95	2.73
	outliers (%)	0.25	0.50
Average B-factor		66.46	39.54
protein		67.97	38.61
thiosulfate		73.25	-
monoolein		44.20	51.12
water		-	34.03

Table 2. k_a, k_d, and K_D values of the interactions between YeeE and YeeD proteins

	k_a (1/μM・s)	k_d (1/s)	K_D (μM)
WT	0.017 ± 0.0029	0.027 ± 0.0029	1.6 ± 0.20
K8A	0.0089 ± 0.0011	0.037 ± 0.0019	4.3 ± 0.61
E9A	0.0060 ± 0.00058	0.027 ± 0.0021	4.6 ± 0.22
E15A	0.0075 ± 0.0013	0.071 ± 0.033	9.5 ± 4.2
V16A	0.017 ± 0.0016	0.093 ± 0.023	5.6 ± 0.86
C17A	*	*	*
L38A	0.018 ± 0.0013	0.032 ± 0.0030	1.7 ± 0.055
V39A	0.0058 ± 0.00033	0.032 ± 0.00058	5.4 ± 0.30
D42A	**	**	**
Y43A	0.0082 ± 0.00095	0.16 ± 0.017	20 ± 2.1
L45A	0.029 ± 0.0016	0.035 ± 0.0040	1.2 ± 0.10
E48A	0.017 ± 0.010	0.14 ± 0.20	4.5 ± 6.2
R49A	0.0090 ± 0.0014	0.12 ± 0.16	17 ± 23
E63A	0.018 ± 0.00026	0.030 ± 0.0013	1.7 ± 0.074

*: The affinity of YeeD C17A derivative for YeeE was too low, and the value could not be calculated accurately.

**: The YeeD D42A sample contained a significant amount of intermolecular S-S dimers (fig. S2F); therefore, the value was omitted here.

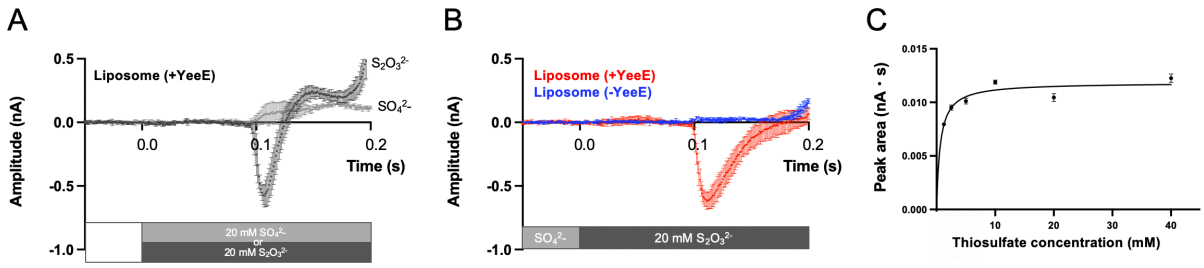

Fig. 1. Thiosulfate ion transport activity of *St*YeeE-reconstituted liposomes. (**A**) Selective uptake of thiosulfate ion by *St*YeeE. *St*YeeE-reconstituted liposomes were used for the measurement using the SSM method. The non-activation buffer, lacking any sulfur-related ions, was exchanged with buffer containing either 20 mM $Na_2S_2O_3$ or 20 mM Na_2SO_4 at 0.0 s. (**B**) YeeE-dependent negative current changes. Liposomes with and without *St*YeeE were used. The non-activation buffer containing 20 mM Na_2SO_4 was exchanged with buffer containing 20 mM $Na_2S_2O_3$ instead of Na_2SO_4 at 0.0 s. The current values from three measurements were standardized based on the average values from -0.05 to 0.0 s, and then the mean values from the three measurements were calculated. Error bars indicate the SD (standard deviation). (**C**) Thiosulfate concentration dependency of the uptake activity. The current changes were monitored in the same manner as in (B), except for the concentration of thiosulfate and sulfate ions (1.25, 2.5, 5, 10, 20, and 40 mM). The negative peak area values (nA・s) from three measurements were calculated and plotted with the SD. The plot was fitted with Michaelis–Menten equation, and V_{max} was estimated as 0.01184 nA・s and K_m as 0.6261 mM.

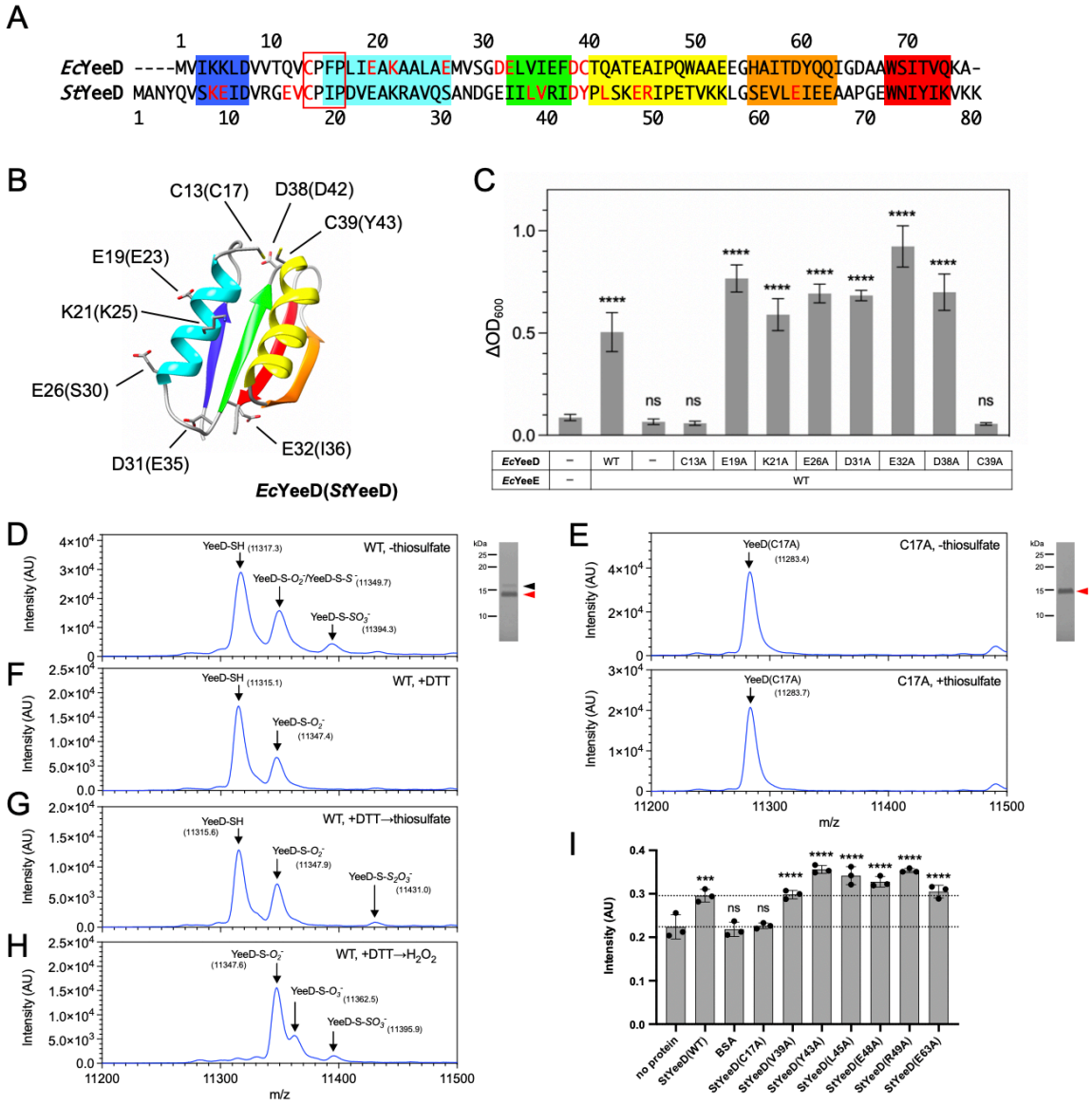

Fig. 2. Characterization of YeeD functions in vivo and in vitro.

(**A**) Sequence alignment of *Ec*YeeD and *St*YeeD. The regions of α-helices and β-strands predicted by AlphaFold2 in (B) are highlighted with colors. Red text indicates amino acid residues that were mutated in this study. The conserved CPxP motif is enclosed in a red rectangle. (**B**) Cartoon model of AlphaFold2-predicted structure of *Ec*YeeD. α-helices and β-strands are colored as in (A). The side chains of amino acid residues mutated for growth complementation analysis in (C) are shown as stick models. Corresponding amino acid residues from *St*YeeD are also indicated in parentheses. (**C**) Growth complementation assay of Δ*cysPUWA* Δ*yeeE* (DE3) cells, depending on *Ec*YeeE and *Ec*YeeD expression from plasmids. The mean values of increased OD_{600} (ΔOD_{600}) after

24 h are shown. Error bars represent the SD from three measurements. Statistical significance compared with the Δ*cysPUWA* Δ*yeeE* (DE3) cells possessing an empty vector was determined using one-way analysis of variance (ANOVA) followed by Dunnett's multiple comparisons tests (****, $p < 0.0001$; ns, not significant). (**D**) CBB-stained SDS-PAGE gel and mass spectrometry of purified *St*YeeD(WT). Red and black arrowheads indicate the major and minor bands of purified WT *St*YeeD, respectively. In mass spectrometry, three major peaks corresponding to -SH, -S-O_2^-/-S-S^-, and -S-SO_3^- were detected. (**E**) CBB-stained SDS-PAGE gel and mass spectrometry of purified *St*YeeD(C17A) (upper) and 500 μM thiosulfate-treated *St*YeeD(C17A) (lower). In mass spectrometry, a single peak was observed. **(F)** Mass spectrometry of DTT-reduced *St*YeeD(WT). **(G)** Mass spectrometry of 500 μM thiosulfate-treated *St*YeeD after DTT-reduction. **(H)** Mass spectrometry of *St*YeeD oxidized by hydrogen peroxide after DTT-reduction. (**I**) Measurement of in vitro enzymatic activity of *St*YeeD. Fluorescence intensity changes derived from an H_2S-detectable fluorescent probe, HSip-1, in the presence of thiosulfate (500 μM) were measured using a series of purified *St*YeeD derivatives in 10 mM Tris-HCl pH 8.0, 300 mM NaCl, and 70 μM β-ME. Mean values of three experiments are shown. Error bars represent SD. Statistical significance compared with samples containing no protein was determined using one-way ANOVA followed by Dunnett's multiple comparisons tests (***, $p < 0.001$; ****, $p < 0.0001$; ns, not significant). Dashed lines indicate the mean values of no-protein samples and *St*YeeD(WT).

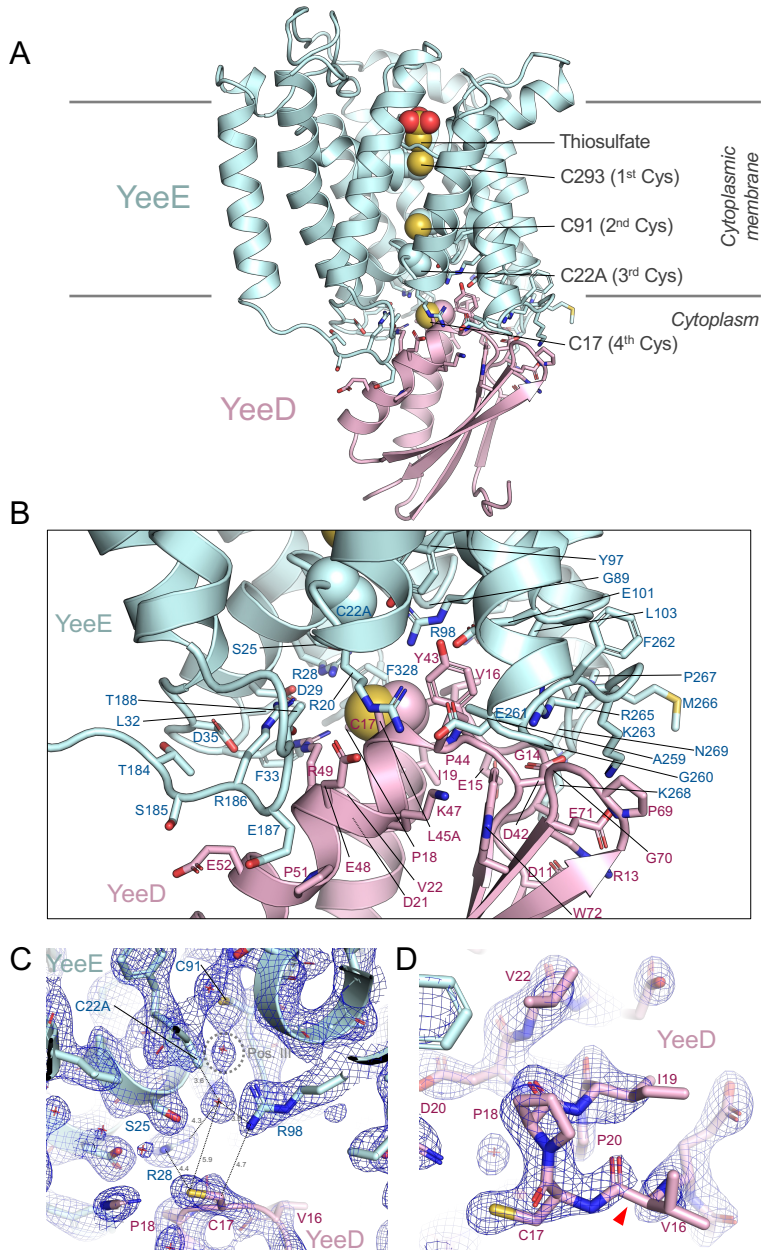

Fig. 3. Crystal structure of *St*YeeE-*St*YeeD complex (PDB ID 8K1R).
(A) Cartoon model of *St*YeeE(C22A)-YeeD(L45A). The side chains of amino acid residues on the contact surfaces between *St*YeeE and *St*YeeD are shown as stick models. The side chains of the conserved cysteine positions are shown in the spheres model. The thiosulfate ion in the *St*YeeE(C22A)-YeeD model (PDB ID 8J4C) was superimposed as spheres model. (**B**) Close-up view of the contact region. (**C**) 2Fo-Fc electron density map at 1.5 δ of the border region around C22A in *St*YeeE and C17 in *St*YeeD. Position III is a previously proposed thiosulfate-binding site. The red stars indicate water molecules. (**D**) 2Fo-Fc electron density map at 1.3 δ around the CPxP motif. The red arrowhead indicates where electron density map is faint.

930

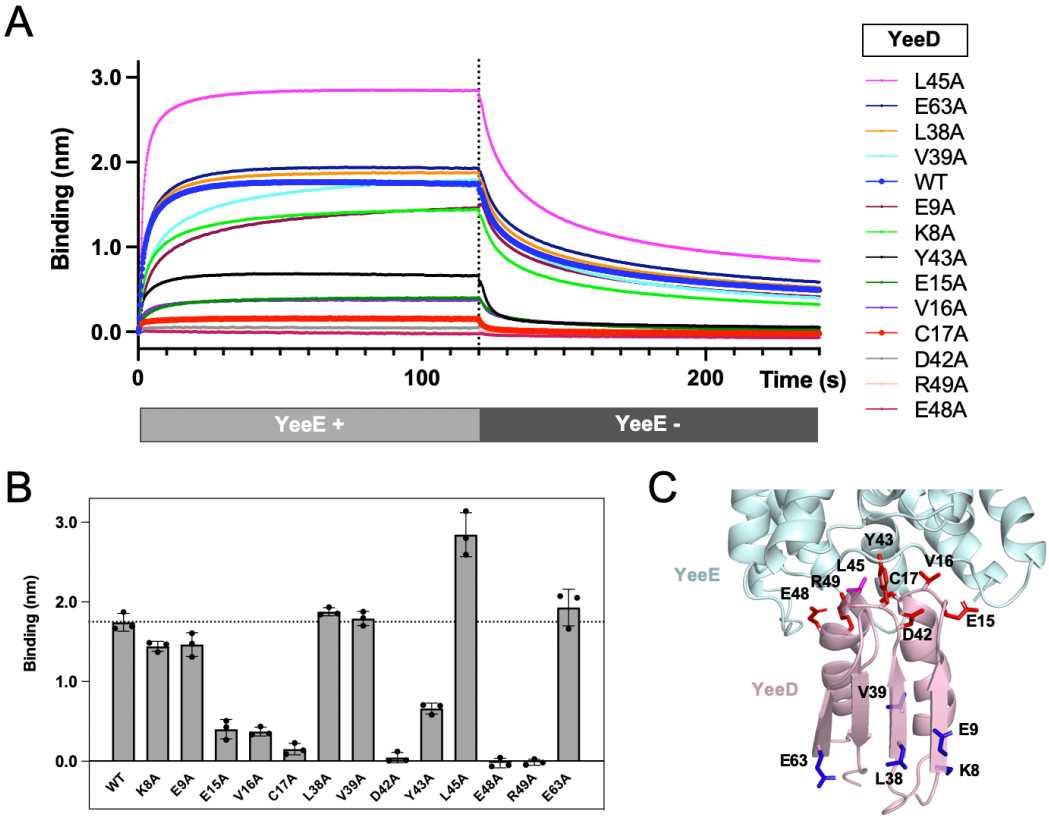

931

932 **Fig. 4. Interaction between *St*YeeE and *St*YeeD.**

933 (**A**) Real-time detection by the BLI method of association and dissociation of *St*YeeE
934 with/from solidified *St*YeeD and its derivatives with Octet buffer (20 mM Tris-HCl pH
935 8.0, 300 mM NaCl, 0.1% (w/v) DDM, 1 mM β-ME) Each line shows the mean value of
936 three measurements. The dashed line indicates the 120-s point where *St*YeeD-solidified
937 biosensors were submerged in the YeeE-free buffer. (**B**) Mean values of *St*YeeE binding
938 to solidified *St*YeeD at 120 s. Error bars show the SD of three measurements. The
939 dashed line indicates the mean value of *St*YeeD(WT). (**C**) Mutation site mapping on the
940 crystal structure of *St*YeeE-YeeD complex (PDB ID 8J4C). The side chains of mutated
941 amino acid residues in (A) are shown as stick models. Magenta, blue, and red residues
942 indicate that those Ala-substituted mutants showed increased, similar, and reduced
943 binding affinity, respectively, compared to WT.

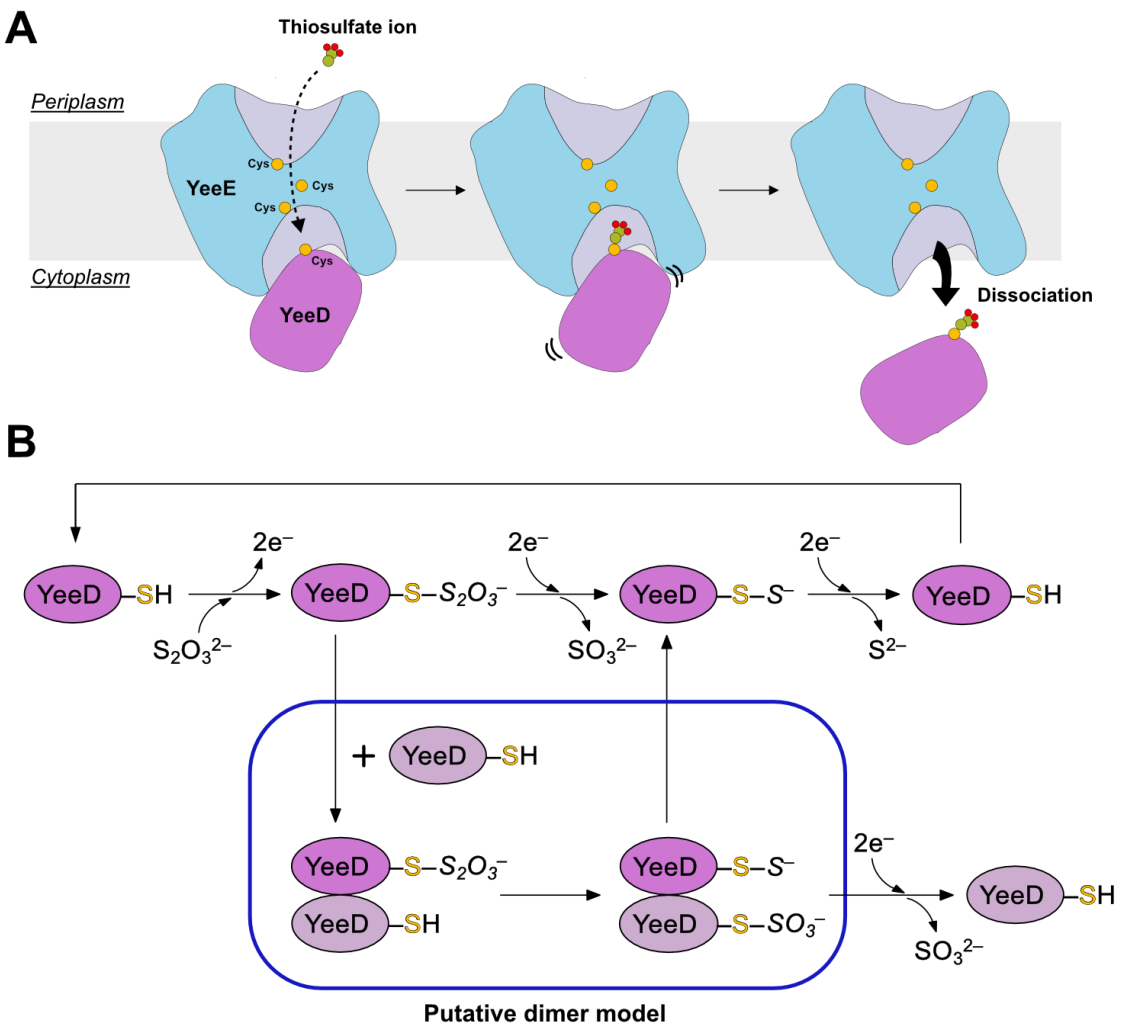

944

945 **Fig. 5. Model of uptake and decomposition of thiosulfate ion by YeeE and YeeD.**
946 (**A**) Uptake of a thiosulfate ion by YeeE and YeeD. The thiosulfate ion is relayed by
947 conserved cysteine residues of YeeE and binds to the conserved cysteine residue of
948 YeeD. After that, the association of YeeD with YeeE is destabilized. YeeD then
949 dissociates from YeeE and decomposes the thiosulfate. (**B**) Thiosulfate decomposition
950 by YeeD. First, thiosulfate binds directly to the conserved cysteine residue of YeeD.
951 Next, sulfide ion (SO_3^{2-}) is released. Finally, sulfite ion (S^{2-}) is released. In the blue box,
952 a putative dimerization model of *St*YeeD is shown.